Article

Water-Driven Structural Transformation in Cobalt Trimesate Metal-Organic Frameworks

Jayashree Ethiraj [1,2,*], Vinayagam Surya [1], Parasuraman Selvam [1,3,4,*] and Jenny G. Vitillo [5,*]

[1] National Centre for Catalysis Research, Department of Chemistry, Indian Institute of Technology Madras, Chennai 600 036, India; suryavinayak11@gmail.com

[2] Center for Nanoscience and Technology, Chennai Institute of Technology, Kundrathur, Chennai 600 069, India

[3] School of Chemical Engineering and Analytical Science, The University of Manchester, Manchester M13 9PL, UK

[4] Department of Chemical and Process Engineering, University of Surrey, Guildford, Surrey GU2 7XH, UK

[5] Department of Science and High Technology and INSTM, University of Insubria, Via Valleggio 9, 22100 Como, Italy

* Correspondence: jayashreee@citchennai.net (J.E.); selvam@iitm.ac.in (P.S.); jg.vitillo@gmail.com (J.G.V.)

Abstract: We report on the synthesis and the characterization of a novel cobalt trimesate metal-organic framework, designated as KCL-102. Powder X-ray diffraction pattern of KCL-102 is dominated by a reflection at $10.2°$ (d-spacing = 8.7 Å), while diffuse reflectance UV-Vis spectroscopy indicates that the divalent cobalt centers are in two different coordination geometries: tetrahedral and octahedral. Further, the material shows low stability in humid air, and it transforms into the well-known phase of hydrous cobalt trimesate, $Co_3(BTC)_2 \cdot 12H_2O$. We associated this transition with the conversion of the tetrahedral cobalt to octahedral cobalt.

Keywords: MOFs; solvothermal synthesis; cobalt trimesate; $Co_3(BTC)_2 \cdot 12H_2O$

1. Introduction

In the past 25 years of research on metal-organic frameworks (MOFs) [1], MOFs set a benchmark as a highly porous class of materials with characteristic physical and chemical properties. MOFs were extensively studied for gas adsorption [2–4], gas separation [3,5], gas storage [6], gas sensing [7], heterogeneous catalysis [8,9], luminescence [10], and drug delivery [11,12]. In recent studies, MOFs were widely studied and regarded as active materials for supercapacitors owing to their flexible structure and outstanding porosity, which also includes electrochemical applications [13] drawing attention to electronic properties and dielectric response [14]. Cobalt-based MOFs were studied for various applications, such as for removal of Pb ions from aqueous solution [15] to materials for post-combustion CO_2 capture [16]. Nevertheless, among the most intriguing applications for Co-MOFs, there is the low-dimensional magnetism. Divalent cobalt centers in MOFs offer the opportunity to realize low dimensional magnetism studies [17,18]. In fact, the different arrangements that cobalt ions can have in the MOFs metal nodes (chains [19], single atoms [20], paddle wheel [21]) allows one to obtain materials with very peculiar magnetic properties. The possibility to design the materials with such precision at the atomic scale is unprecedented for magnetic materials. Cobalt oxides are among the most studied materials for water splitting [22]. Co-O species in MOFs were exploited for the same aim; in fact, cobalt MOFs were reported to be active catalysts for hydrogen evolution reactions [23] and oxygen evolution and reduction reactions [24]. Co-MOFs started to gain attention in energy sectors as electrode materials for supercapacitors, and they can be classified into two main groups: (i) MOFs as excellent precursors for synthesis of porous transition metal oxides, carbon, or metal oxides embedded in porous carbon matrices [25,26]; (ii) MOFs directly used as electrode materials for supercapacitors due to their porosity and metal cations providing the accommodation space of

electrolytes and the redox active sites [27,28]. Nevertheless, relatively few cobalt MOFs are reported to date, e.g., ZIF-67 (cobalt-2methylimidazoate framework, [20]), Co-ZIF-9 (cobalt-benzimidazolate framework, [29]), DUT-8 ($Co_2(NDC)_2DABCO$, NDC = 2,6-napththalene dicarboxylate, DABCO = 1,4-diazabicyclo[2.2.2]octane, [30]), Co-MOF-74 and CPO-27-Co (cobalt-2,5 dihydroxyterephthate framework, [31]), Co-UTSA-16 ($K_2Co_3(cit)_2$, cit = fully dehydroxylated citrate anion, [32,33]), Co-BDP (cobalt-1,4-benzenedipyrazolate framework, [34]), $Co_2(BDC)_2(DABCO)$ (BDC = benzenedicarboxylate, [30]), and $Co_2Cl_2(BTDD)$ (BTDD = bis(1H-1,2,3- triazolo[4,5-b],[4′,5′-i])dibenzo[1,4]dioxin, [19]).

Cobalt trimesates (Co-BTC, BTC = benzene-1,3,5-tricarboxylate) were reported previously. A search on the Cambridge Structural Database (CSD) indicates the presence of 27 deposited structures with cobalt and trimesate [35]. The first material reported as a metal-organic framework by Yaghi et al. in 1995 was a cobalt trimesate [36]. Other cobalt trimesates were reported since then for very different applications [37–45]. Among them, $Co_3(BTC)_2 \cdot 12H_2O$ [46] is particularly interesting for energy related applications. Tan et al. [47] suggested $Co_3(BTC)_2 \cdot 12H_2O$ as a catalyst for CO oxidation, and Yaqoob et al. [48] proved $Co_3(BTC)_2 \cdot 12H_2O$ and its nanocomposites with rGO to be promising for oxygen evolution reaction. This material showed also a very high thermal stability, reported to be up 450 °C [47]. On the other hand, a mixed nickel and cobalt 1,3,5-benzenetricarboxylate (Ni-Co-BTC) was proposed as anode material for lithium-ion batteries [49].

Herein, we report a solvothermal process to obtain a Co-BTC MOF (**KCL-102**) which has a quite different powder X-ray diffraction (PXRD) pattern than the reported Co-BTCs. We investigated the stability of this novel Co-BTC after contact with air and water by using PXRD, scanning electron microscopy (SEM), thermogravimetry (TG), and diffuse ultraviolet-visible spectroscopy (DRUV-Vis). **KCL-102** is not stable in moisture. Nevertheless, unlike most parts of MOFs that become amorphous upon contact with water, it undergoes a phase transformation to another crystalline phase, non-porous Co-BTC, the previously reported $Co_3(BTC)_2 \cdot 12H_2O$ [46].

2. Materials and Methods

All the chemicals were purchased from Sigma Aldrich and were used without any further purification. Table 1 lists three different synthesis parameters for the preparation of **KCL-102**. **KCL-102** was synthesized using benzene-1,3,5-tricarboxylic acid (BTC) and cobalt nitrate hexahydrate in 1:2 (molar ratio). At first, BTC was dissolved in 100 mL DMF and 50 mL Millipore water mixture. The cobalt source was then added to the solution and stirred until it completely dissolved (~15 min). The solution was transferred to a 250 mL Teflon lined autoclave and kept in preheated oven at 140 °C for 1–2 h. The resulting precipitate was filtered and dried at 50 °C for 2 h, washed with DMF, and dried again at 50 °C for 2 h.

Table 1. Experimental conditions used for the synthesis of **KCL-102** (BTC = 1,3,5-benzenetricarboxylic acid, DMF = dimethyl-formide, T = temperature).

| Item	$Co(NO_3)_2 \cdot 6H_2O$ (g)	BTC (g)	DMF (mL)	H_2O (mL)	T (°C)	Reaction Time (min)
Batch 1	1.4551	0.5250	100	50	140	120
Batch 2	2.9102	1.0508	100	50	140	120
Batch 3	1.4551	0.5250	100	50	140	80

PXRD patterns were recorded using a Rigaku Miniflex tabletop diffractometer equipped with a Cu X-ray tube ($K\alpha_1$ = 1.540562 Å) with fixed tube voltage of 30 kV and output current of 15 mA; it was also equipped with a graphite monochromator. The diffraction patterns were collected in Bragg Brentano geometry in the 3–70° 2θ range with step size of 0.02°. The simulated powder diffraction pattern of $Co_3(BTC)_2 \cdot 12H_2O$ was obtained by using the structure reported in Ref. [46] by employing the program Mercury 2020.2.0 [50]. SEM images were obtained with an FEI 400 instrument operated at 30 kV. TGA was carried out

on a TAQ600 (TA Instruments) with a ramp rate of 10 °C/min from room temperature to 700 °C in nitrogen or in dry air flow using an alumina pan.

Infrared (IR) spectra were recorded on JASCO spectrometer in transmittance mode in the range of 4000 to 400 cm^{-1} using a deuterated triglycine sulfate detector on self-supported pellets obtained by diluting the MOF powder in KBr. DRUV-Vis spectra were recorded on a JASCO 650 spectrometer. BaSO$_4$ was used as the reference standard. The spectra were acquired in air with loose powders diluted in pure BaSO$_4$ placed inside the standard powder cell of the instrument.

3. Results and Discussion

Three batches of **KCL-102** were synthesized (see Table 1), and all the samples showed similar PXRD patterns (Figure 1a), indicating the good reproducibility of the synthesis. The reaction yield was not dependent on the reaction conditions used, being 35–40% in all cases. The reaction time was significantly shorter compared to the typical Co$_3$(BTC)$_2$·12H$_2$O synthesis (20–24 h, [46,47]). All the patterns reported in Figure 1a,b were equivalent, and they were all different from the patterns reported for other metal trimesates. The structures used for the comparison were obtained by search in articles collection databases [24,35–46,48,51–54] and in the Cambridge Structural Database (CCSD, [55]) using as a query in ConQuest one cobalt atom bound to one oxygen atom of a BTC linker and coordinated to two additional oxygen atoms through a single bond. The most intense reflection of the pattern was centered at 10.2°, corresponding with a *d*-spacing of 8.7 Å. No variation was observed in the diffraction patterns after DMF washing (blue line, Figure 1b).
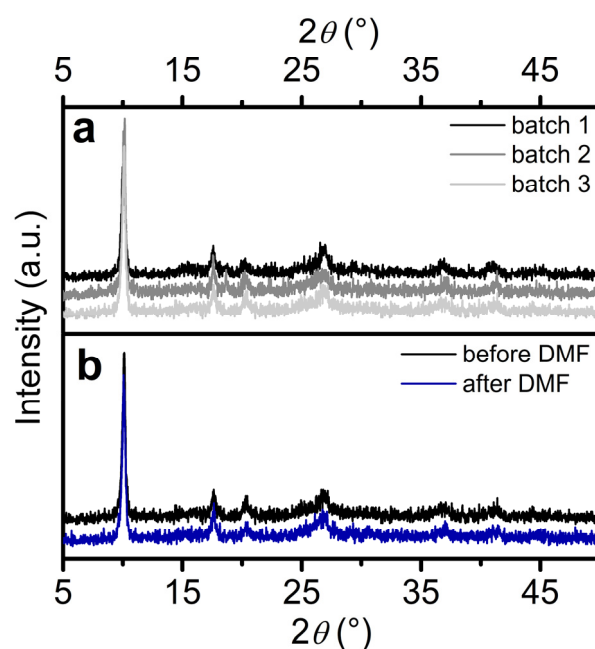

Figure 1. PXRD diffractograms of **KCL-102**. (**a**) Diffraction patterns of as-synthesized **KCL-102** in various batches using different reaction conditions (see Table 1). (**b**) Diffraction patterns of the as-synthesized **KCL-102** before and after washing with DMF.

KCL-102 is not stable in air for a prolonged time. The material dried at 50 °C and left in the air was found to undergo to a phase transformation that was completed in one week, and the resulting sample was designated as **KCL-102-air** following. This structural transformation was ascribable to moisture (see below), and the conversion was much faster upon contacting **KCL-102** with a droplet of water and drying it in the air (**KCL-102-H$_2$O**). A similar observation was previously noticed for MOFs in the presence of protic solvents [56]. **KCL-102-air** and **KCL-102-H$_2$O** were fully equivalent from their characterization. In the following, only the results obtained for **KCL-102-air** are reported.

The phase transformation was accompanied by a change in the color from violet (**KCL-102**) to pale pink (**KCL-102-air** and **KCL-102-H$_2$O**). Likewise, the color change was also observed in the reaction mixture left in the air after a few days. A first attempt to measure the surface area of **KCL-102** was made, thermally treating the sample in vacuum at 100 °C and 150 °C. Unfortunately, the desorption of a large amount of solvent (likely DMF) from the sample to the measurement cell hindered the isotherm collection. Future studies should be aimed at the determination of a washing procedure for the removal of DMF from the sample, e.g., using low boiling solvents.

The diffraction patterns recorded for the as-made **KCL-102** (blue line) and **KCL-102-air** (light magenta) are presented in Figure 2a. It can be seen from this figure that the two patterns were significantly different. Noteworthy, the diffraction pattern of **KCL-102-air** corresponded to the Co$_3$(BTC)$_2$·12H$_2$O pattern (see Figure 2a), a non-porous MOF reported formerly by Yaghi et al. [46] that was suggested as a catalyst for CO oxidation [47] and a promising candidate for oxygen evolution reaction [48]. The structure of Co$_3$(BTC)$_2$·12H$_2$O as in Ref. [46] is reported in Figure 2b. Nevertheless, some additional reflections were identified in the **KCL-102-air** that were not present in the Co$_3$(BTC)$_2$·12H$_2$O pattern at 9.3°, 12.5°, 23.2°, and 23.5°. Among them, the most intense were the reflections at 9.3° and 12.5°. These reflections could not be indexed as belonging to the expected products from **KCL-102** decomposition (Co(OH)$_2$, Co$_3$O$_4$, and trimesic acid) or to any other reported Co trimesates (Refs. [35–46]). Although these peaks could be related to an additional Co trimesate phase, we suggest that they were associated with the formation of mesopores due to framework collapse, as already reported for other MOFs. Unfortunately, the presence of a significant amount of DMF did not allow us to record the nitrogen isotherm for **KCL-102-air** or to verify this hypothesis.
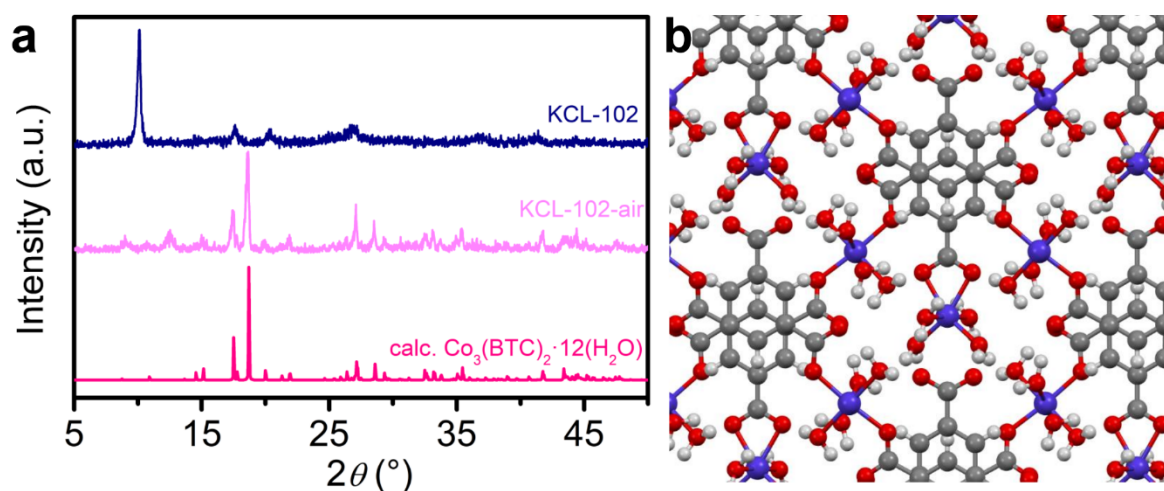
Figure 2. (**a**) XRD patterns of DMF-washed **KCL-102** (blue line) and after leaving **KCL-102** in the air for one week (**KCL-102-air**, light pink line). The calculated pattern of Co$_3$(BTC)$_2$·12H$_2$O using the structure reported in Ref. [46] is also shown for comparison (dark pink line). (**b**) View along [001] of Co$_3$(BTC)$_2$·12H$_2$O structure as reported in Ref. [46]. Color code: violet (Co), red (O), grey (C), white (H).

Figure 3a displays the SEM image of the **KCL-102**. It can be seen from this image that the material exhibited a well-defined cuboid structure with size ranging from 15 to 20 μm. On the other hand, **KCL-102-air** (Figure 3b) showed a significantly altered morphology after contact with moisture/air leading to distributed sizes predominantly with needle-shaped particles.
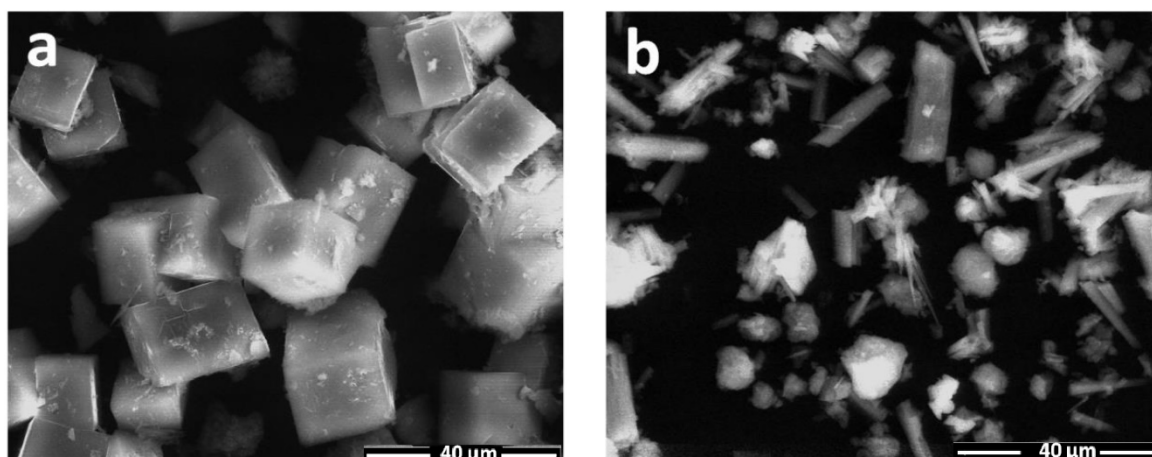
Figure 3. SEM images of (**a**) KCL-102 and (**b**) KCL-102-air.

The thermal stability of **KCL-102** and **KCL-102-air** in a flow of dry air or nitrogen was compared by using thermogravimetry (TG). The data obtained for **KCL-102** and **KCL-102-air** are reported in parts a and b of Figure 4, respectively. Regarding **KCL-102,** it was not possible to assign the different steps in the TG trace, as its chemical formula is unknown (Figure 4a). We were limited to observing that **KCL-102** TG trace was not dependent on the reaction environment up to 350 °C (Figure 4a), with temperature corresponding to about 10% weight loss. This result indicated a significant thermal stability of **KCL-102**. The weight loss up to 350 °C was continuous without abrupt changes, and it was likely associated with solvent (water and DMF) and unreacted linker desorption from the MOF pores. Material decomposition started at 350 °C and 450 °C in air and nitrogen, respectively, corresponding to structural water desorption and material decomposition.

The TG traces of the hydrated cobalt trimesate, **KCL-102-air**, in a flow of dry air (dashed line) or nitrogen (solid line) are reported in Figure 4b. Regarding TG collected under nitrogen atmosphere, it can be seen from this figure that a substantial weight loss between 100–400 °C (~26 wt%) could be attributed to the removal of the coordinated water molecules. This result was similar to that reported by Crane et al. [38]. The plateau extended up to 450 °C, indicating the larger thermal stability of $Co_3(BTC)_2 \cdot 12H_2O$ compared to **KCL-102**. The second stage weight loss (~30 wt%) evidenced in the temperature range 450–525 °C could be associated with framework collapse leading to the formation of $Co(OH)_2$ (34.5 wt%) followed by a continuous weight loss to Co_3O_4 (29.8 wt%).

As expected, a similar behavior was observed for the sample heated in air (dashed line in Figure 4b), however, with the onset temperatures shifted to lower values. In this case, a plateau was reached at 420 °C, and that was maintained at least up to 700 °C. The observed weight loss (64 wt%) was close to the one expected for the formation of Co_3O_4.

We investigated **KCL-102** using infrared (FTIR) and UV-Vis spectroscopy in order to gain some knowledge on details of **KCL-102** structure. Figure 5 shows the vibration modes of **KCL-102** (blue line) and **KCL-102-air** (pink line) in comparison with the spectra of the trimesic acid (black line) and of MIL-100(Fe), an iron trimesate [57] (brown line). MIL-100(Fe) spectrum was used a standard for the quick identification of carboxylate band and unreacted carboxylic acid groups in **KCL-102** and **KCL-102-air**. The IR spectrum of **KCL-102-air** matched well with the spectrum reported by Yaghi et al. for $Co_3(BTC)_2 \cdot 12H_2O$ [46]. In the 3600–2800 cm^{-1} region, the spectra of **KCL-102** and **KCL-102-air** were clearly dominated by a large band due to the solvent molecules (water and DMF), both structural and physisorbed solvent molecules. The relative intensity of these bands was larger in **KCL-102-air** than in **KCL-102** because of the larger hydration degree of the former. IR absorption bands of the BTC linker were observed in the 1800–400 cm^{-1} range. For comparison, the spectra of a trimesate salt (MIL-100(Fe), brown line) and of trimesic acid (black line) are also reported in Figure 5. The absorption bands in the ranges 1700–1500 cm^{-1}

and 1500–1300 cm^{-1} corresponded to ν_{asym}(COO) and ν_{sym}(COO). These bands were remarkably similar to the ones observed in the iron trimesate. No signals were observed that could be associated with unreacted carboxylic acid. The signal observed at 1681 cm^{-1} was likely associated with DMF [58]. The band centered at 758 cm^{-1} in **KCL-102** spectrum was previously assigned to ν(C-H) bending mode in HKUST-1, a copper trimesate [59]. Alves et al. [60] reported the FT-IR spectra of nanoparticles of Co_3O_4: they observed the bands at 567 and 665 cm^{-1} which were related to the Co-O stretching vibrations. For Co_2O_3 nanoparticles, the vibrational band was observed at 560 cm^{-1} owing to the Co–O stretching vibration mode, and 668 cm^{-1} was the bridging vibration of the O–Co–O bond. The higher band at 668 cm^{-1} was normal for Co^{2+}–O vibration in a tetrahedral site, and the lower band 560 cm^{-1} was accredited to the Co^{3+}–O vibration at the octahedral site [61]. In case of Co-BTC, at a lower wavenumber region, two vibrational modes centered at 554 and 455 cm^{-1} were observed. The vibrational modes corresponding to cobalt oxides falls at 554 cm^{-1} could be assigned to Co-O stretching vibrational modes. Co-O stretching vibrational mode at 554 cm^{-1} in **KCL-102** was highly perturbed in **KCL-102-air**, hinting at the changes in coordination around Co^{2+}.

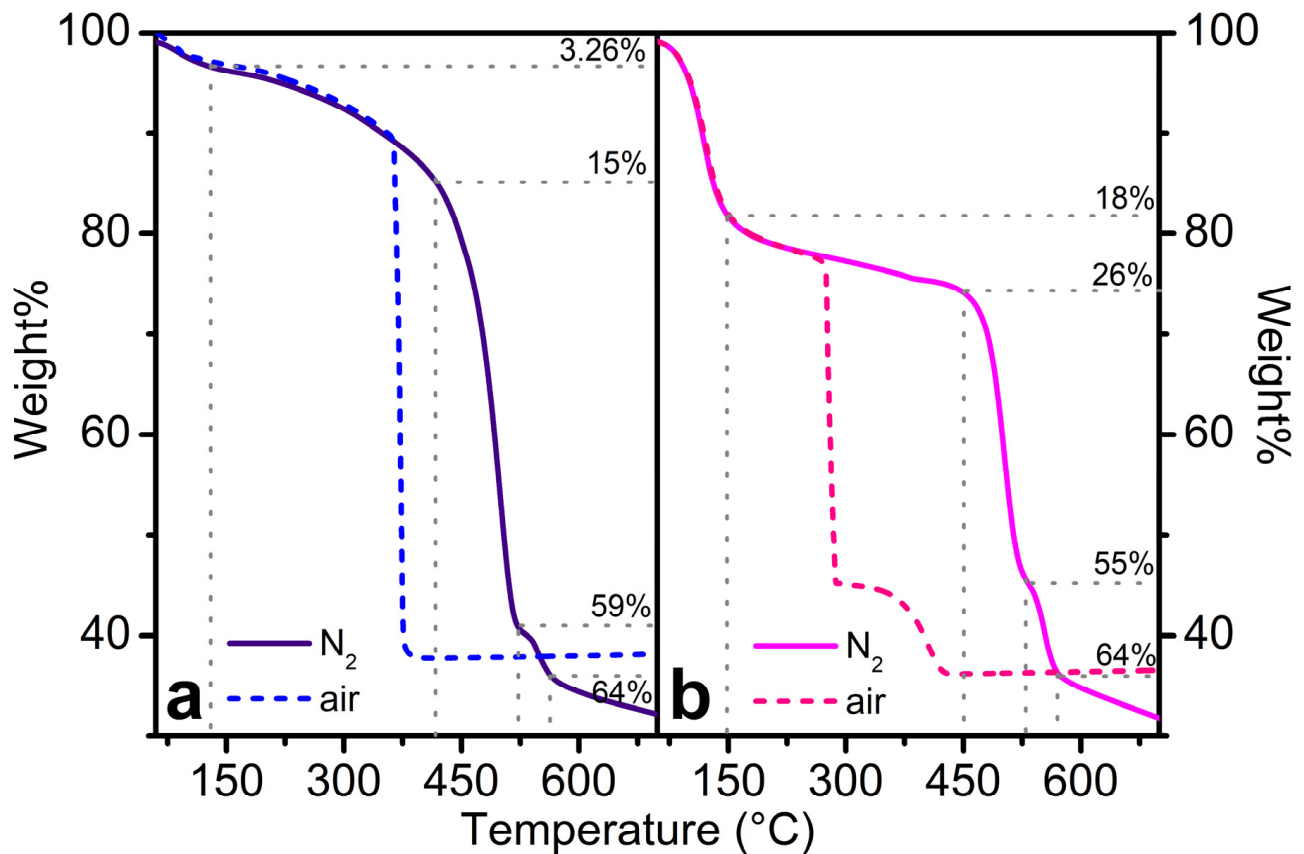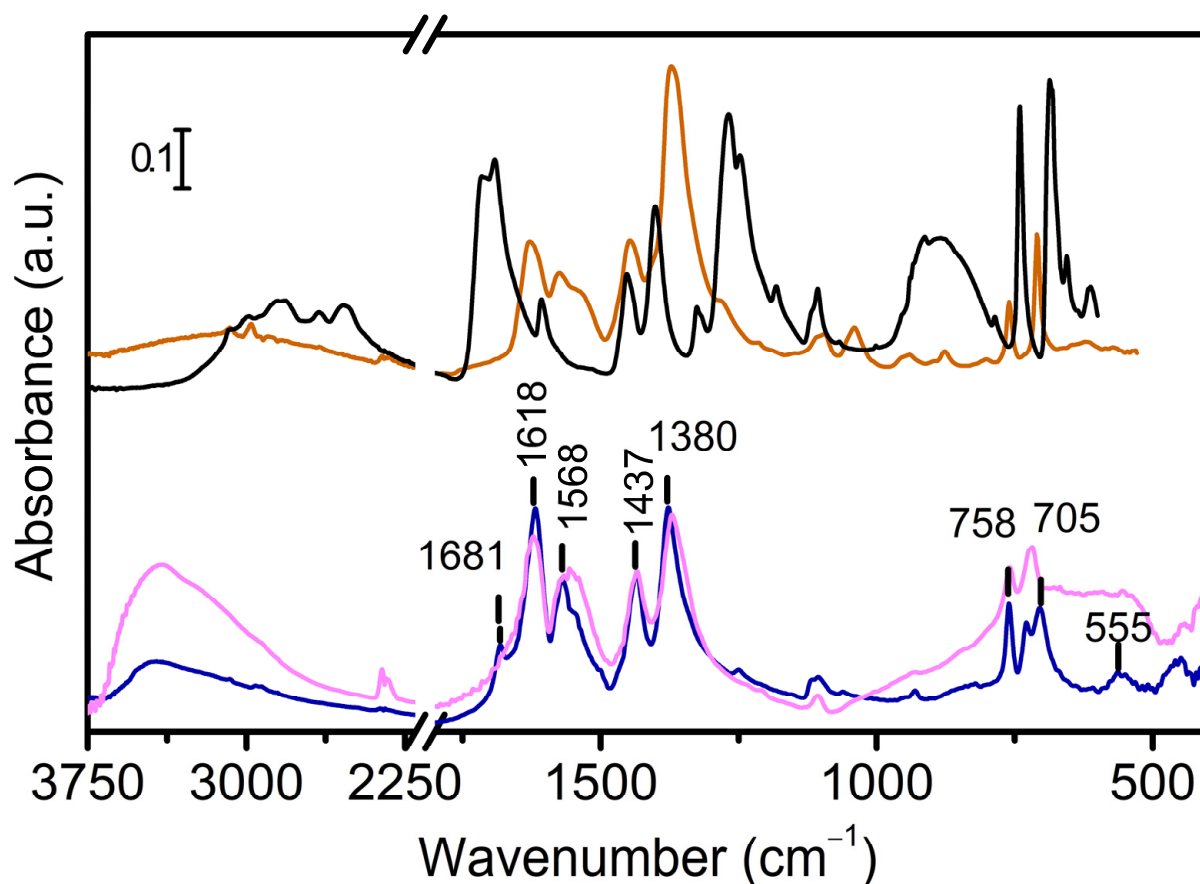**Figure 4.** TG traces of (**a**) **KCL-102** and (**b**) **KCL-102-air** in a flow of dry air and N$_2$.

Figure 5. FT-IR spectrum of **KCL-102** (blue line) recorded in air right after synthesis compared to the spectrum of **KCL-102-air** (light pink), trimesic acid (black line), and of another trimesate based MOF (MIL-100(Fe), unpublished data, brown line). For additional characterization of this MIL-100(Fe) sample, please refer to Ref. [57].

Diffuse reflectance UV-vis (DR-UV-vis) provides information on the oxidation state and on the coordination of the cobalt, that is, the number of the ligands, their symmetry, and their chemical nature. Moreover, oxidation states different than 2+ cannot be excluded a priori for cobalt. As mentioned above, the phase transition caused a change in the color of the powder from violet of **KCL-102** (Figure 6c) to pink of **KCL-102-air** (Figure 6d). A synthetized $Co_3(BTC)_2 \cdot 12H_2O$ was a pink powder [44]. A violet color was, in general, associated with the copresence in cobalt-based materials of Co centers in both octahedral and tetrahedral coordination [32]. This was, for example, the case of UTSA-16, the spectra of which were characterized by two peaks at 527 and 566 nm due to d-d transitions in Co(II) in octahedral and tetrahedral geometry (see black line in Figure 6b and discussion in Ref. [32]). In Figure 6b (green curve), another Co(II) based MOF, ZIF-67, having all the cobalt centers in tetrahedral coordination is reported as a reference. The spectra of KCL-102 samples before and after the exposure to air confirmed the divalent state of the cobalt centers. **KCL-102** spectrum (blue curve in Figure 6a) showed two bands at 520 and 578 nm that were then assigned to d-d transitions of Co(II) centers in octahedral and tetrahedral geometry in analogy to UTSA-16. **KCL-102** peaks were less defined than UTSA-16, suggesting a heterogeneous nature of the two families of cobalt centers. The $Co_3(BTC)_2 \cdot 12H_2O$ structure is known [46]. Cobalt ions in the materials were all in octahedral coordination, although of two different kinds: one coordinated with four H_2O molecules and two O belonging to the same COO- group, while the other one coordinated with four H_2O molecules and two O belonging to two different COO- groups (Figure 6e). Accordingly, **KCL-102-air** spectrum (pink spectrum in Figure 6a) was characterized by a complex broad band centered at 540 nm. The low intensity signal at 578 nm could be associated with residual **KCL-102**.
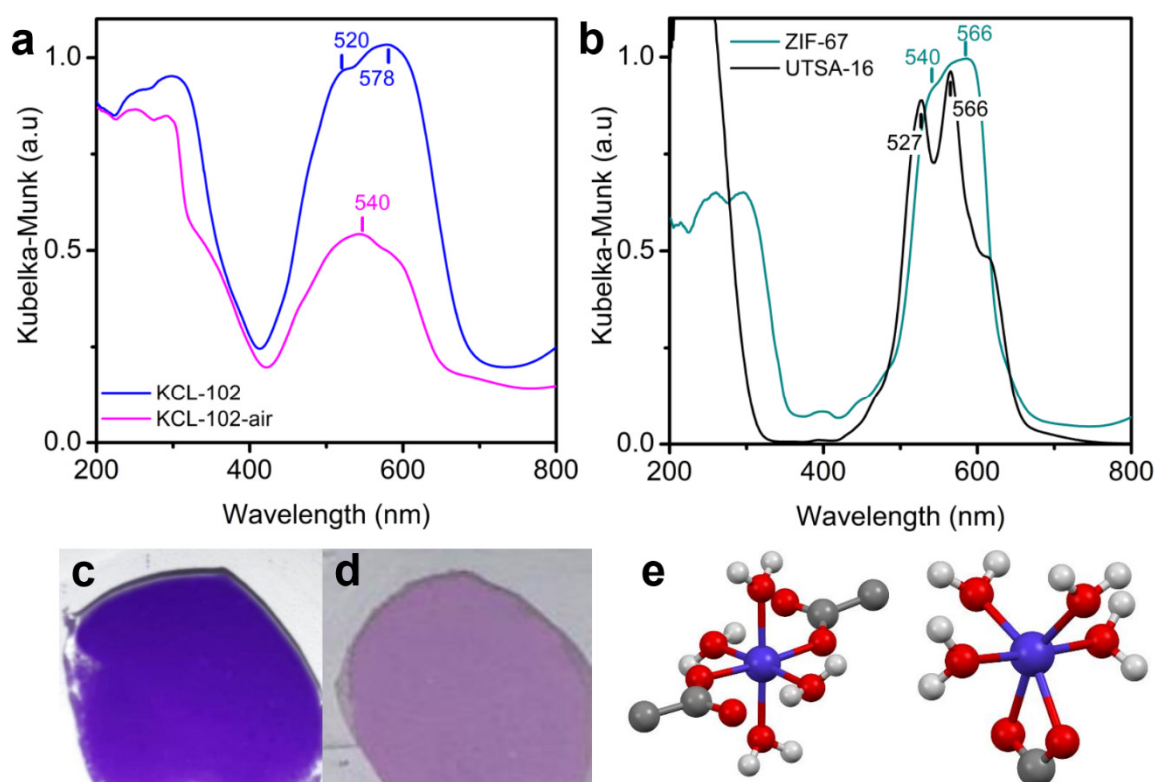
Figure 6. (**a**) DRUV-vis spectra of **KCL-102** (blue line) and **KCL-102-air** (magenta). (**b**) DRUV-Vis spectra of ZIF-67 (green line) and UTSA-16 (black line, from Ref. [32]). All the spectra were recorded in the air. (**c,d**) Photographs of the **KCL-102** (**c**) and the **KCL-102-air** (**d**) samples. (**e**) First coordination environment of cobalt centers in **KCL-102-air** as in the experimental structure reported in Ref. [46]. Color atom code: violet (Co), red (O), grey (C), white (H).

4. Conclusions

We report here a novel cobalt trimesate, **KCL-102**, and we verified the high reproducibility of its synthesis protocol. **KCL-102** is characterized by a large thermal stability in nitrogen and dry air (up to 350 °C), as verified by thermogravimetry. Nevertheless, **KCL-102** is unstable in air, and it undergoes a slow phase transformation (for about a week) to its hydrated form, $Co_3(BTC)_2 \cdot 12H_2O$. This transformation is very quick in direct contact with water. Furthermore, unlike several other MOFs, **KCL-102** does not become amorphous upon hydration, but it is converted to a well-known crystalline phase, $Co_3(BTC)_2 \cdot 12H_2O$. Various physico-chemical characterization results indicate the presence of tetrahedrally and octahedrally coordinated Co(II) in the **KCL-102** framework, while in $Co_3(BTC)_2 \cdot 12H_2O$, only octahedrally coordinated Co(II) are present, suggesting a water-induced phase transformation that causes the conversion of the tetrahedral Co(II) to octahedral Co(II). At this juncture, it is to be noted here that the main difference between the synthesis protocols of **KCL-102** and $Co_3(BTC)_2 \cdot 12H_2O$ is the shorter reaction time of the former, being 2 h for **KCL-102** and 20–24 h for $Co_3(BTC)_2 \cdot 12H_2O$. The presence of cobalt centers having an oxidation state different than 2+ was excluded in this study based on the UV-Vis measurements, although these results should be confirmed also by means of other techniques such as X-ray photoelectron spectroscopy (XPS), X-ray absorption near edge spectroscopy (XANES), or superconducting quantum interference device (SQUID).

Future investigations should be aimed at the determination of the **KCL-102** structure and surface area and to its testing for the several energy-related applications where cobalt-based MOFs are known to be excellent in regard to water harvesting, heat exchangers, oxygen reduction reaction (ORR), oxygen evolution reaction (OER), and CO and other oxidation reactions [54].

References

1. Ralph, F.; Stefano, C.; Seth, M.C.; Wei, Y.; Hexiang, D.; Vincent, G.; Mohamed, E.; David, G.M.; David, F.-J.; Hao, L.; et al. 25 years of Reticular Chemistry. *Angew. Chem. Int. Ed.* **2021**. [CrossRef]
2. Alhamami, M.; Doan, H.; Cheng, C.-H. A Review on Breathing Behaviors of Metal-Organic-Frameworks (MOFs) for Gas Adsorption. *Materials* **2014**, *7*, 3198–3250. [CrossRef]
3. Li, H.; Wang, K.; Sun, Y.; Lollar, C.T.; Li, J.; Zhou, H.-C. Recent advances in gas storage and separation using metal-organic frameworks. *Mater. Today* **2018**, *21*, 108–121. [CrossRef]
4. Wanigarathna, D.K.J.A.; Gao, J.; Liu, B. Metal organic frameworks for adsorption-based separation of fluorocompounds: A review. *Mater. Adv.* **2020**, *1*, 310–320. [CrossRef]
5. Songolzadeh, M.; Soleimani, M.; Ravanchi, M.T.; Songolzadeh, R. Carbon Dioxide Separation from Flue Gases: A Technological Review Emphasizing Reduction in Greenhouse Gas Emissions. *Sci. World J.* **2014**. [CrossRef]
6. Sumida, K.; Rogow, D.L.; Mason, J.A.; McDonald, T.M.; Bloch, E.D.; Herm, Z.R.; Bae, T.-H.; Long, J.R. Carbon Dioxide Capture in Metal-Organic Frameworks. *Chem. Rev.* **2012**, *112*, 724–781. [CrossRef]
7. Li, H.-Y.; Zhao, S.-N.; Zang, S.-Q.; Li, J. Functional metal-organic frameworks as effective sensors of gases and volatile compounds. *Chem. Soc. Rev.* **2020**, *49*, 6364–6401. [CrossRef]
8. Pascanu, V.; Miera, G.G.; Inge, A.K.; Martin-Matute, B. Metal-Organic Frameworks as Catalysts for Organic Synthesis: A Critical Perspective. *J. Am. Chem. Soc.* **2019**, *141*, 7223–7234. [CrossRef]
9. Wang, Q.; Astruc, D. State of the Art and Prospects in Metal-Organic Framework (MOF)-Based and MOF-Derived Nanocatalysis. *Chem. Rev.* **2020**, *120*, 1438–1511. [CrossRef] [PubMed]
10. Cui, Y.; Yue, Y.; Qian, G.; Chen, B. Luminescent Functional Metal-Organic Frameworks. *Chem. Rev.* **2012**, *112*, 1126–1162. [CrossRef]
11. Cao, J.; Li, X.; Tian, H. Metal-Organic Framework (MOF)-Based Drug Delivery. *Curr. Med. Chem.* **2020**, *27*, 5949–5969. [CrossRef]
12. Wang, L.; Zheng, M.; Xie, Z. Nanoscale metal-organic frameworks for drug delivery: A conventional platform with new promise. *J. Mater. Chem. B* **2018**, *6*, 707–717. [CrossRef]
13. Punde, N.S.; Rawool, C.R.; Rajpurohit, A.S.; Karna, S.P.; Srivastava, A.K. Hybrid Composite Based on Porous Cobalt-Benzenetricarboxylic Acid Metal Organic Framework and Graphene Nanosheets as High Performance Supercapacitor Electrode. *ChemistrySelect* **2018**, *3*, 11368–11380. [CrossRef]
14. Ryder, M.R.; Dona, L.; Vitillo, J.G.; Civalleri, B. Understanding and Controlling the Dielectric Response of Metal-Organic Frameworks. *ChemPlusChem* **2018**, *83*, 308–316. [CrossRef] [PubMed]
15. Shooto, N.D.; Ayawei, N.; Wankasi, D.; Sikhwivhilu, L.; Dikio, E.D. Study on cobalt metal organic framework materials as adsorbent for lead ions removal in aqueous solution. *Chem. Asian J.* **2016**, *28*, 277–281. [CrossRef]
16. Danaci, D.; Bui, M.; Mac Dowell, N.; Petit, C. Exploring the limits of adsorption-based CO2 capture using MOFs with PVSA—from molecular design to process economics. *Mol. Syst. Des. Eng.* **2020**, *5*, 212–231. [CrossRef]
17. Dong, J.-L.; Xie, F.; Du, J.-Q.; Lan, H.-M.; Yang, R.-X.; Wang, D.-Z. Cobalt MOFs base on benzimidazol and varied carboxylate ligands with higher capacitance for supercapacitors and magnetic properties. *J. Solid State Chem.* **2019**, *279*, 120917. [CrossRef]
18. Dubskikh, V.A.; Lysova, A.A.; Samsonenko, D.G.; Lavrov, A.N.; Kovalenko, K.A.; Dybtsev, D.N.; Fedin, V.P. 3D Metal–Organic Frameworks Based on Co(II) and Bithiophendicarboxylate: Synthesis, Crystal Structures, Gas Adsorption, and Magnetic Properties. *Molecules* **2021**, *26*, 1269. [CrossRef] [PubMed]
19. Rieth, A.J.; Dincă, M. Controlled Gas Uptake in Metal–Organic Frameworks with Record Ammonia Sorption. *J. Am. Chem. Soc.* **2018**, *140*, 3461–3466. [CrossRef]
20. Ethiraj, J.; Palla, S.; Reinsch, H. Insights into high pressure gas adsorption properties of ZIF-67: Experimental and theoretical studies. *Microporous Microporous Mater.* **2020**, *294*. [CrossRef]

21. Marri, S.R.; Chauhan, N.; Tiwari, R.K.; Kumar, J.; Behera, J.N. Two novel 3D-MOFs (Ca-TATB and Co-HKUST): Synthesis, structure and characterization. *Inorg. Chim. Acta* **2018**, *478*, 8–14. [CrossRef]
22. Ghosh, S.; Bloom, B.P.; Lu, Y.; Lamont, D.; Waldeck, D.H. Increasing the Efficiency of Water Splitting through Spin Polarization Using Cobalt Oxide Thin Film Catalysts. *J. Phys. Chem. C* **2020**, *124*, 22610–22618. [CrossRef]
23. Han, W.; Li, M.; Ma, Y.; Yang, J. Cobalt-Based Metal-Organic Frameworks and Their Derivatives for Hydrogen Evolution Reaction. *Front. Chem.* **2020**, *8*. [CrossRef] [PubMed]
24. Tripathy, R.K.; Samantara, A.K.; Behera, J.N. A cobalt metal-organic framework (Co-MOF): A bi-functional electro active material for the oxygen evolution and reduction reaction. *Dalton Trans.* **2019**, *48*, 10557–10564. [CrossRef]
25. Pang, H.; Gao, F.; Chen, Q.; Liu, R.; Lu, Q. Dendrite-like Co3O4 nanostructure and its applications in sensors, supercapacitors and catalysis. *Dalton Trans.* **2012**, *41*, 5862–5868. [CrossRef] [PubMed]
26. Liu, B.; Shioyama, H.; Akita, T.; Xu, Q. Metal-Organic Framework as a Template for Porous Carbon Synthesis. *J. Am. Chem. Soc.* **2008**, *130*, 5390–5391. [CrossRef]
27. Yang, J.; Xiong, P.; Zheng, C.; Qiu, H.; Wei, M. Metal–organic frameworks: A new promising class of materials for a high performance supercapacitor electrode. *J. Mater. Chem. A* **2014**, *2*, 16640–16644. [CrossRef]
28. Liu, X.; Shi, C.; Zhai, C.; Cheng, M.; Liu, Q.; Wang, G. Cobalt-Based Layered Metal–Organic Framework as an Ultrahigh Capacity Supercapacitor Electrode Material. *ACS Appl. Mater. Interfaces* **2016**, *8*, 4585–4591. [CrossRef] [PubMed]
29. Ozturk, Z.; Hofmann, J.P.; Lutz, M.; Mazaj, M.; Logar, N.Z.; Weckhuysen, B.M. Controlled Synthesis of Phase-Pure Zeolitic Imidazolate Framework Co-ZIF-9. *Eur. J. Inorg. Chem.* **2015**, 1625–1630. [CrossRef]
30. Tu, T.N.; Nguyen, K.D.; Nguyen, T.N.; Thanh, T.; Phan, N.T.S. New topological Co-2(BDC)(2)(DABCO)as a highly active heterogeneous catalyst for the amination of oxazoles via oxidative C-H/N-H couplings. *Catal. Sci. Technol.* **2016**, *6*, 1384–1392. [CrossRef]
31. Valenzano, L.; Civalleri, B.; Sillar, K.; Sauer, J. Heats of Adsorption of CO and CO₂ in Metal-Organic Frameworks: Quantum Mechanical Study of CPO-27-M (M = Mg, Ni, Zn). *J. Phys. Chem. C* **2011**, *115*, 21777–21784. [CrossRef]
32. Masala, A.; Vitillo, J.G.; Bonino, F.; Manzoli, M.; Grande, C.A.; Bordiga, S. New insights into UTSA-16. *Phys. Chem. Chem. Phys.* **2016**, *18*, 220–227. [CrossRef]
33. Lawson, S.; Al-Naddaf, Q.; Krishnamurthy, A.; Amour, M.S.; Griffin, C.; Rownaghi, A.A.; Knox, J.C.; Rezaei, F. UTSA-16 Growth within 3D-Printed Co-Kaolin Monoliths with High Selectivity for CO2/CH4, CO2/N-2, and CO2/H-2 Separation. *ACS Appl. Mater. Interfaces* **2018**, *10*, 19076–19086. [CrossRef] [PubMed]
34. Taylor, M.K.; Runcevski, T.; Oktawiec, J.; Gonzalez, M.I.; Siegelman, R.L.; Mason, J.A.; Ye, J.; Brown, C.M.; Long, J.R. Tuning the Adsorption-Induced Phase Change in the Flexible Metal Organic Framework Co(bdp). *J. Am. Chem. Soc.* **2016**, *138*, 15019–15026. [CrossRef]
35. Cambridge Structural Database. Available online: https://www.ccdc.cam.ac.uk/ (accessed on 10 June 2021).
36. Yaghi, O.M.; Li, G.; Li, H. Selective binding and removal of guests in a microporous metal–organic framework. *Nature* **1995**, *378*, 703–706. [CrossRef]
37. Hamidipour, L.; Farzaneh, F. Cobalt metal organic framework as an efficient heterogeneous catalyst for the oxidation of alkanes and alkenes. *React. Kinet. Mech. Catal.* **2013**, *109*, 67–75. [CrossRef]
38. Crane, J.L.; Anderson, K.E.; Conway, S.G. Hydrothermal Synthesis and Characterization of a Metal–Organic Framework by Thermogravimetric Analysis, Powder X-ray Diffraction, and Infrared Spectroscopy: An Integrative Inorganic Chemistry Experiment. *J. Chem. Educ.* **2015**, *92*, 373–377. [CrossRef]
39. Ejegbavwo, O.A.; Berseneva, A.A.; Martin, C.R.; Leith, G.A.; Pandey, S.; Brandt, A.J.; Park, K.C.; Mathur, A.; Farzandh, S.; Klepov, V.V.; et al. Heterometallic multinuclear nodes directing MOF electronic behavior. *Chem. Sci.* **2020**, *11*, 7379–7389. [CrossRef]
40. Zhou, K.; Jiang, F.-L.; Chen, L.; Wu, M.-Y.; Zhang, S.-Q.; Ma, J.; Hong, M.-C. Unprecedented three-level hierarchical entanglement in a coordination polymer. *Chem. Commun.* **2012**, *48*, 12168–12170. [CrossRef]
41. Israr, F.; Chun, D.; Kim, Y.; Kim, D.K. High yield synthesis of Ni-BTC metal–organic framework with ultrasonic irradiation: Role of polar aprotic DMF solvent. *Ultrason. Sonochem.* **2016**, *31*, 93–101. [CrossRef] [PubMed]
42. Horcajada, P.; Serre, C.; Vallet-Regí, M.; Sebban, M.; Taulelle, F.; Férey, G. Metal–Organic Frameworks as Efficient Materials for Drug Delivery. *Angew. Chem. Int. Ed.* **2006**, *45*, 5974–5978. [CrossRef]
43. Nowacka, A.; Briantais, P.; Prestipino, C.; Llabrés i Xamena, F.X. Facile "Green" Aqueous Synthesis of Mono- and Bimetallic Trimesate Metal–Organic Frameworks. *Cryst. Growth Des.* **2019**, *19*, 4981–4989. [CrossRef]
44. Steenhaut, T.; Hermans, S.; Filinchuk, Y. Green synthesis of a large series of bimetallic MIL-100(Fe,M) MOFs. *New J. Chem.* **2020**, *44*, 3847–3855. [CrossRef]
45. Faustini, M.; Kim, J.; Jeong, G.Y.; Kim, J.Y.; Moon, H.R.; Ahn, W.S.; Kim, D.P. Microfluidic Approach toward Continuous and Ultrafast Synthesis of Metal-Organic Framework Crystals and Hetero Structures in Confined Microdroplets. *J. Am. Chem. Soc.* **2013**, *135*, 14619–14626. [CrossRef] [PubMed]
46. Yaghi, O.M.; Li, H.; Groy, T.L. Construction of Porous Solids from Hydrogen-Bonded Metal Complexes of 1,3,5-Benzenetricarboxylic Acid. *J. Am. Chem. Soc.* **1996**, *118*, 9096–9101. [CrossRef]
47. Tan, H.; Liu, C.; Yin, Y.; Wu, J. Simple Preparation of Crystal Co-3(BTC)(2)center dot 12H(2)O and Its Catalytic Activity in CO Oxidation Reaction. *J. Wuhan Univ. Technol. Mater. Sci. Ed.* **2015**, *30*, 71–75. [CrossRef]

48. Yaqoob, L.; Noor, T.; Iqbal, N.; Nasir, H.; Sohail, M.; Zaman, N.; Usman, M. Nanocomposites of cobalt benzene tricarboxylic acid MOF with rGO: An efficient and robust electocatalyst for oxygen evaluation reaction (OER). *Renew. Energy* **2020**, *156*, 1040–1054. [CrossRef]
49. Zheng, W.; Bi, W.; Gao, X.; Zhang, Z.; Yuan, W.; Li, L. A nickel and cobalt bimetal organic framework with high capacity as an anode material for lithium-ion batteries. *Sustain. Energy Fuels* **2020**, *4*, 5757–5764. [CrossRef]
50. Macrae, C.F.; Sovago, I.; Cottrell, S.J.; Galek, P.T.A.; McCabe, P.; Pidcock, E.; Platings, M.; Shields, G.P.; Stevens, J.S.; Towler, M.; et al. Mercury 4.0: From visualization to analysis, design and prediction. *J. Appl. Cryst.* **2020**, *53*, 226–235. [CrossRef]
51. Wu, Y.; Qiu, L.-G.; Wang, W.; Li, Z.-Q.; Xu, T.; Wu, Z.-Y.; Jiang, X. Kinetics of oxidation of hydroquinone to p-benzoquinone catalyzed by microporous metal-organic frameworks M3(BTC)2 [M = copper(II), cobalt(II), or nickel(II); BTC = benzene-1,3,5-tricarboxylate] using molecular oxygen. *Transit. Met. Chem.* **2009**, *34*, 263–268. [CrossRef]
52. Yan, W.; Han, L.-J.; Jia, H.-L.; Shen, K.; Wang, T.; Zheng, H.-G. Three Highly Stable Cobalt MOFs Based on "Y"-Shaped Carboxylic Acid: Synthesis and Absorption of Anionic Dyes. *Inorg. Chem.* **2016**, *55*, 8816–8821. [CrossRef] [PubMed]
53. Xuan, W.; Ramachandran, R.; Zhao, C.; Wang, F. Influence of synthesis temperature on cobalt metal-organic framework (Co-MOF) formation and its electrochemical performance towards supercapacitor electrodes. *J. Solid State Electrochem.* **2018**, *22*, 3873–3881. [CrossRef]
54. Dhakshinamoorthy, A.; Montero Lanzuela, E.; Navalon, S.; Garcia, H. Cobalt-Based Metal Organic Frameworks as Solids Catalysts for Oxidation Reactions. *Catalysts* **2021**, *11*, 95. [CrossRef]
55. Groom, C.R.; Bruno, I.J.; Lightfoot, M.P.; Ward, S.C. The Cambridge Structural Database. *Acta Cryst.* **2016**, *72*, 171–179. [CrossRef]
56. Vitillo, J.G.; Bordiga, S. Increasing the stability of Mg$_2$(dobpdc) metal-organic framework in air through solvent removal. *Mater. Chem. Front.* **2017**, *1*, 444–448. [CrossRef]
57. Simons, M.C.; Vitillo, J.G.; Babucci, M.; Hoffman, A.S.; Boubnov, A.; Beauvais, M.L.; Chen, Z.; Cramer, C.J.; Chapman, K.W.; Bare, S.R.; et al. Structure, Dynamics, and Reactivity for Light Alkane Oxidation of Fe(II) Sites Situated in the Nodes of a Metal–Organic Framework. *J. Am. Chem. Soc.* **2019**, *141*, 18142–18151. [CrossRef]
58. Bonino, F.; Lamberti, C.; Chavan, S.; Vitillo, J.G.; Bordiga, S. Characterization of MOFs. 1. Combined Vibrational and Electronic Spectroscopies. In *Metal Organic Frameworks as Heterogeneous Catalysts*; Llabrés i Xamena, F.X., Gascon, J., Eds.; The Royal Society of Chemistry: Cambridge, UK, 2013; pp. 76–142.
59. Ethiraj, J.; Bonino, F.; Lamberti, C.; Bordiga, S. H2S interaction with HKUST-1 and ZIF-8 MOFs: A multitechnique study. *Microporous Mesoporous Mater.* **2015**, *207*, 90–94. [CrossRef]
60. Alves, I.C.B.; Santos, J.R.N.; Viegas, D.S.S.; Marques, E.P.; Lacerda, C.A.; Zhang, L.; Zhang, J.J.; Marques, A.L.B. Nanoparticles of Fe2O3 and Co3O4 as Efficient Electrocatalysts for Oxygen Reduction Reaction in Acid Medium. *J. Braz. Chem. Soc.* **2019**, *30*, 2681–2690. [CrossRef]
61. Rajeevgandhi, C.; Sathiyamurthy, K.; Guganathan, L.; Savithiri, S.; Bharanidharan, S.; Mohan, K. Experimental and theoretical investigations on the spinel structure of Co(2)O(3)nanoparticles synthesized via simple co-precipitation method. *J. Mater. Sci. Mater. Electron.* **2020**, *31*, 16769–16779. [CrossRef]